Spectroscopy and Femtosecond Dynamics of 7-*N*,*N*-Diethylamino-3-hydroxyflavone. The Correlation of Dipole Moments among Various States To Rationalize the Excited-State Proton Transfer Reaction

Yi-Ming Cheng, Shih-Chieh Pu, Yueh-Chi Yu, Pi-Tai Chou,* Chien-Huang Huang, and Chao-Tsen Chen*

Department of Chemistry, National Taiwan University, Taipei, Taiwan, ROC

Tsung-Hui Li and Wei-Ping Hu*

Department of Chemistry & Biochemistry, National Chung Cheng University, Chia-Yi, Taiwan, ROC

Received: May 24, 2005; In Final Form: October 27, 2005

Comprehensive excitation behaviors of 7-*N*,*N*-diethylamino-3-hydroxyflavone (**I**) have been investigated via steady state, temperature-dependent emission, and fluorescence upconversion to probe the excited-state intramolecular proton transfer (PT) reaction. Upon excitation, **I** undergoes ultrafast ($\ll$120 fs), adiabatic type of charge transfer (CT), so that the dipolar vector in the Franck–Condon excited state is much different from that in the ground state. In polar solvents such as CH_2Cl_2 and CH_3CN, early relaxation dynamics clearly reveals the competitive rates between solvent relaxation and PT dynamics. After reaching thermal equilibrium, a relatively slow, solvent-polarity-dependent rate (a few tens of picoseconds^{-1}) of PT takes places. Firm support of the early relaxation dynamics is rendered by the spectral temporal evolution, which resolves two distinct bands ascribed to CT and PT emission. The results, in combination with ab initio calculations on the dipolar vectors for various corresponding states, led us to conclude that excited-state normal (N*) and excited proton-transfer tautomer (T*) possesses very different dipole orientation, whereas the dipole orientation of the normal ground state (N) is between that of N* and T*. PT is thus energetically favorable at the Franck–Condon excited N*, and its rate is competitive with respect to the solvent relaxation dynamics induced by CT. Unlike the well-known PT system, 4′-*N*,*N*-diethylamino-3-hydroxyflavone,$^{10-19}$ in which equilibrium exists between solvent-equilibrated N_{eq}* and T_{eq}*, N_{eq}* $\rightarrow$ T_{eq}* PT for **I** is a highly exergonic, irreversible process in all solvents studied. Further temperature-dependent studies deduce a solvent-polarity-perturbed energy barrier of 3.6 kcal/mol for the N_{eq}* $\rightarrow$ T_{eq}* PT in CH_3CN. The proposed dipole-moment-tuning PT mechanism with the associated relaxation dynamics is believed to apply to many PT molecules in polar, aprotic solvents.

1. Introduction

The excited-state intramolecular proton transfer (PT)[1] has been considered as one of the most fundamental processes involved in chemical reactions. The PT molecules generally possess either six- or five-membered rings with strong intramolecular hydrogen bonds (HB) between O–H (or N–H) and C=O (or pyridinic nitrogen) groups. For these molecules, the intrinsic proton transfer in the $^1\pi\pi^*$ state[2] is essentially barrierless in nonpolar solvents[3] and may proceed either during periods of low-frequency vibrational motions associated with the hydrogen bonds[4] or ballistically so that the coherent motion can be resolved upon ultrashort pulse excitation.[5]

Recently, based on differences in dipole moments between electronically excited normal and PT tautomer states, a fundamental issue has been raised regarding the solvent polarity tuning PT reaction.[6,7] Considering the case in which molecules exhibit dual properties that incorporate both excited-state intramolecular charge transfer (CT) and PT in character,[8,9] there exists a possible large difference in dipole moment (in either orientation or magnitude) between excited normal (μ^*_N) and proton-transfer

tautomer species (μ^*_T) associated with CT and PT, respectively. Accordingly, the normal and tautomer equilibrium polarizations might be far separated such that the relative energetics between normal and tautomer is expected to be a function of solvent polarization coordinate. On the basis of a large difference in dipole moment and hence in electron density distribution between N* and T* states, one may thus consider N* $\rightarrow$ T* as a prototypical proton transfer-coupled charge transfer type of reaction. Accordingly, the long-range polarization interaction may theoretically results in a solvent-induced barrier channeling into the proton-transfer reaction. As a result, solvent polarity perturbation may play an important role in modifying the PT dynamics.

A seminal proton-transfer-coupled charge-transfer system should be credited to 4′-*N*,*N*-dilkylamino-3-hydroxyflavones (4DHF) (see Scheme 1).[10-14] Recently, investigation of 4DHF has been revitalized through probing the early relaxation dynamics in the femtosecond regime.[15-17] Via the spectral temporal evolution reconstructed from fluorescence upconversion, in combination with theoretical approaches,[17] we concluded that the normal excited state of 4DHF, N*, possessing CT properties, is greatly different in the dipolar vector from that of

* To whom correspondence should be addressed. E-mail: chop@ntu.edu.tw.

SCHEME 1:   Structures of Various 3-Hydroxyflavone Derivatives and the Proposed Lewis Structures of N, N*, and T* States for I (see text for the definition)

4'-N,N-dialkylamino-3-hydroxyflavone

I : R = H
Ia : R = CH$_3$

N

N*

T* (or T)
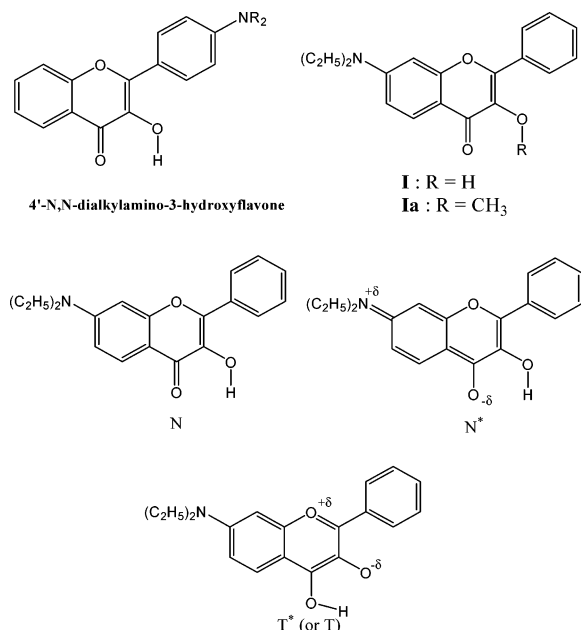
the proton-transfer tautomer state (T*). Conversely, the dipolar vector between T* and normal ground state (N) is similar. Thus, at the Franck–Condon excited N*, PT is energetically favorable, and its rate is competitive with respect to the solvent relaxation dynamics. After reaching the solvent equilibration, there exists an equilibrium between N* and T* states in, for example, CH$_3$-CN, and both forward and reversed PT dynamics are associated with a solvent-induced barrier. The latter equilibrium type of PT has been firmly supported in numerous reports based on steady state,[10−14] picosecond,[18,19] and femtosecond[15,16] approaches.

The core of this CT/PT-coupled mechanism lies in the dynamics of PT being mainly governed by relative dipolar vectors among N, N*, and T*. The weak coupling between N* and T* solvent-polarized potential energy surface induces an appreciable barrier, which then channels into the overall PT dynamics. As for an extension to generalize the dipolar vector tuning mechanism, gaining further insight into other CT/PT systems is demanding. Recently, in a short communication,[6] we have unveiled the design of a new relevant system, 7-*N*,*N*-diethylamino-3-hydroxyflavone (**I**, see Scheme 1), possessing dipole orientation quite different from 4DHF, and have subsequently examined the associated steady state and population relaxation dynamics. Yet, detailed solvent polarity tuning proton-transfer-coupled charge-transfer reactions for **I**, especially the early relaxation dynamics, in which rates of solvent relaxation and PT may be strongly competitive, have not been explored. Herein, we report comprehensive studies on solvent-polarity-dependent spectroscopy and dynamics for **I** and its methoxy derivative, 7-*N*,*N*-diethylamino-3-methoxyflavone (**Ia**). Supplementary support is also provided by temperature-dependent dynamics and theoretical approaches. The results led us to conclude that despite the highly energetically allowed PT process in **I**, the associated reaction dynamics is mainly governed by the solvent polarity due to the separated equilibrium configuration between N* and T* as well as relevant dipolar vectors among N, N*, and T*. We thus deem that the dipolar vector tuning mechanism elaborated in the following sections may apply to numerous PT systems in polar, aprotic solvents.

2. Experimental Section

The various solvents used in the spectroscopic and dynamic measurements were of spectragrade quality (Merck Inc.) and used right after the fractional distillation, in which any contaminations from the protic solvent impurity had been removed by adding suitable drying reagents. Steady-state absorption and emission spectra were recorded by a Hitachi (U-3310) spectrophotometer and an Edinburgh (FS920) fluorimeter, respectively. Pico-nanosecond lifetime and the femtosecond fluorescence upconversion measured were performed using a time-correlated single photon counting technique and a femtosecond optically gated system, respectively, which have been described in previous reports.[7,20] For both pico- and femtosecond time-resolved measurements, the polarization of the pump laser was set at the magic angle (54.7°) with respect to that of the probe laser (or detecting system) to eliminate the fluorescence anisotropy. A variable temperature unit (Specac, P/N 21525) was used to carry out the temperature-dependent studies, for which a range of temperatures from 300 to 77 K can be achieved with an accuracy of ±0.2 °C.

Theoretical calculations were performed using the Gaussian 03 program.[21] The ground (S$_0$) state molecular geometry and dipole moments of **I** and **II**, and their proton-transfer tautomers were calculated using the Hartree–Fock theory with a 6-31G-(d′,p′) basis set. The corresponding molecular geometry and dipole moments at the S$_1$ excited states were calculated using the CI Singles (CIS) theory[22] with the same basis set. The dipole moments of **I** and **II** at the ground-state geometry on the S$_1$ state (vertical excitation) were also calculated at the CIS/6-31G-(d′,p′) level. The nature of the stationary points was also ascertained by harmonic vibrational frequency analysis in both the ground and excited states.

3. Results

3.1. Steady-State Approaches. The provision of a steady-state background is necessary to facilitate comprehension of the following discussion regarding time-resolved and theoretical approaches. Figures 1 depicts the steady-state absorption and emission spectra of **I** and **Ia**, respectively, in various solvents. In all solvents applied, the absorption peak in **I** exhibits a bathochromic shift of 15−20 nm with respect to **Ia**, the result of which can be rationalized by the intramolecular hydrogen bond-enhancing π electron delocalization. Furthermore, with increases in the solvent polarity (cf. CH$_2$Cl$_2$ and CH$_3$CN), a hypsochromic shift in the absorption peak wavelength was observed for both **I** and **Ia**. The results can be rationalized by the S$_0$ → S$_1$ absorption in both **I** and **Ia** manifested by a charge-transfer character incorporating electron donor (diethylamine) and acceptor (carbonyl oxygen). As a result, upon excitation, dipolar changes (either in magnitude or in orientation) on both **I** and **Ia** were expected, resulting in an energetically unfavorable solvated configuration and hence a hypsochromic shift in the absorption spectra. In cyclohexane, **I** exhibits a dominant 560-nm emission band, the peak frequency of which is Stokes shifted by ∼8460 cm^{-1} with respect to the S$_0$ → S$_1$ (ππ*) absorption. In comparison, **Ia**, which is generally treated as a non-PT model due to the lack of the O−H proton, reveals a normal emission maximized at ∼410 nm. Accordingly, it is unambiguous to assign the 560-nm emission for **I** in cyclohexane to origins in the proton-transfer tautomer. However, note that for **I** in cyclohexane there appears a rather small, but nonnegligible normal emission with a peak wavelength at ∼405 nm (see Figure 1A, vide infra).
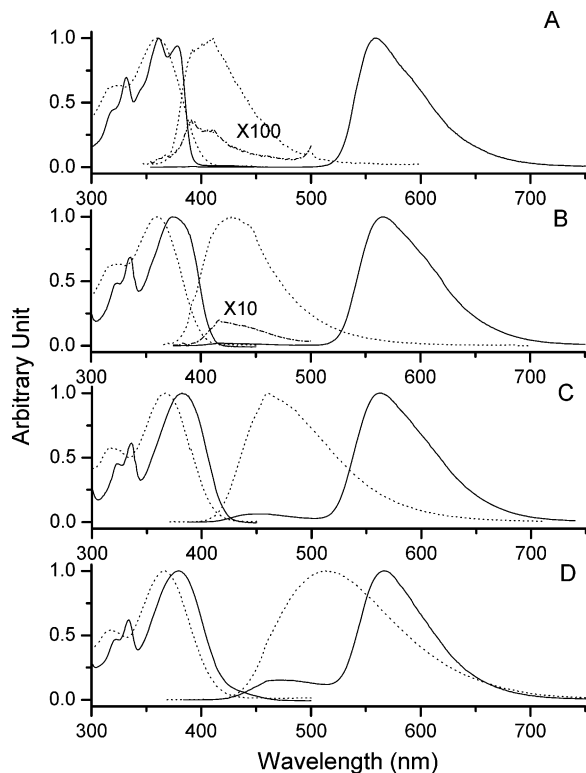
Figure 1. The absorption and emission spectra of **I** (solid line) and **Ia** (dashed line) in cyclohexane (A), benzene (B), dichloromethane (C), and acetonitrile (D) at 298 K.

Upon increases in the solvent polarity, dual emission, consisting of a short (F$_{ct}$) and a long (F$_{pt}$) wavelength band, becomes obvious in compound **I**. While the F$_{pt}$ band is nearly solvent-polarity-independent, the F$_{ct}$ band exhibits strong solvent-polarity-dependence, being shifted from 425 nm (in benzene) to 480 nm (in CH$_3$CN). The entire dual emission originating from a common ground-state species is ascertained by the same fluorescence excitation spectra throughout the monitored wavelengths of 420−700 nm, which are also effectively identical with the absorption spectrum. In comparison, as shown in Figure 1, **Ia** reveals a single emission band, and its peak wavelength is strongly dependent on the solvent polarity. The results clearly indicate that the corresponding state giving emission for **I** (the F$_{ct}$ band) or **Ia** is subject to large dipolar changes with respect to the ground state. Experimentally, the magnitude of dipolar change can be estimated by a method incorporating the emission solvatochromic shift. If the dipole moments of the solute are approximated by a point dipole in the center of a spherical cavity with a radius a_0, on the basis of small solvent-dependent absorption properties and negligence of the solute polarizability, one obtains the following relationship

$$\tilde{\nu}_f = \tilde{\nu}_f^{vac} - \frac{2(\vec{\mu}_e - \vec{\mu}_g)^2}{hca_0^3}\Delta f \qquad (1)$$

where $\tilde{\nu}_f$ and $\tilde{\nu}_f^{vac}$ are the spectral positions (in cm^{-1}) of the solvation-equilibrated fluorescence maxima, the value extrapolated to the diluted gas-phase, respectively, $\vec{\mu}_g$ and $\vec{\mu}_e$ are the dipole moment vectors of the ground and excited states, and Δf is the solvent polarity parameter function and is generally expressed as $\Delta f = (\epsilon - 1)/(2\epsilon + 1)$ where ϵ denotes the static dielectric constant of the solvent. As shown in Figure 2, the plot of the peak frequency as a function of Δf for **I** (F$_{ct}$ emission band) and **Ia** is sufficiently linear and slopes as large as −13969
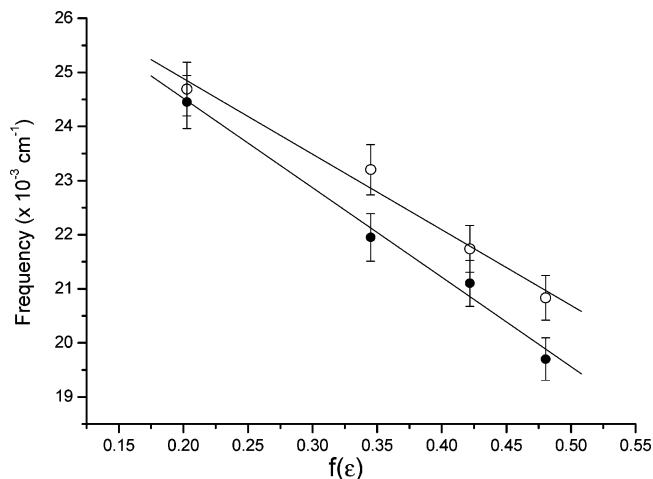

Figure 2. Static emission maxima as a function of solvent polarity $f(\epsilon)$ for **I** (open circle), **Ia** (solid circle).
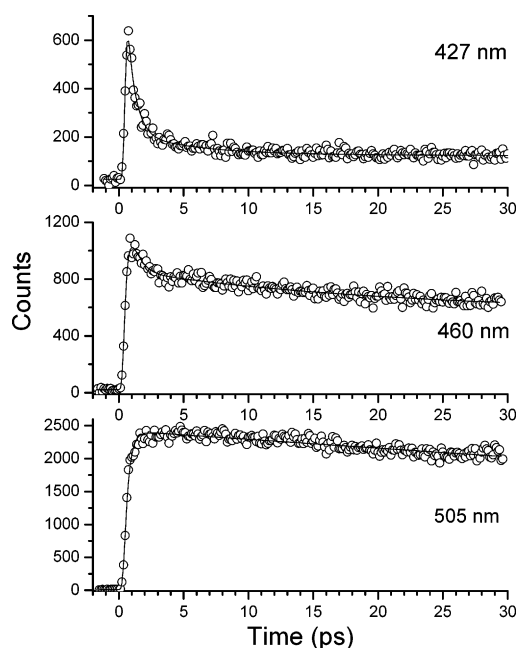

Figure 3. Time-resolved sum frequency signal of fluorescence and gate pulse (760 nm) for **Ia** in dichloromethane. The solid lines express the corresponding best-fitted curves.

and −16525 cm^{-1} are calculated for **I** and **Ia**, respectively, consistent with its assignment of the charge-transfer emission. a_0 in eq 1 was further estimated to be 5.31 Å (**I**) and 5.59 Å (**Ia**) via the Hartree−Fock method with 6-31G(d′,p′) basis sets. Accordingly, the change in dipole moment between ground and excited states is deduced to be 14.4 and 16.9 D for **I** (the F$_{ct}$ band) and **Ia**, respectively. In a sharp contrast, for the proton-transfer emission (the F$_{pt}$ band) in **I**, the change in dipole moment with respect to the ground state is as small as 4.3 D (not shown here).

3.2. Time-Resolved Approaches. *Relaxation Dynamics in Ia.* Prior to any further discussion on **I**, the relaxation dynamics of **Ia**, in which only CT takes place, are presented here in order to delineate the observed relaxation dynamics for **I** in a straightforward manner later.

In cyclohexane, the emission of **Ia** appears with a response-limited rise (<150 fs), followed by a single-exponential population decay component of $\tau_f \sim 70$ ps that is independent of the monitored wavelength. Figures 3 and 4 show the time-resolved fluorescence spectra of **Ia** in CH$_2$Cl$_2$ and CH$_3$CN, respectively.

7-*N*,*N*-Diethylamino-3-hydroxyflavone

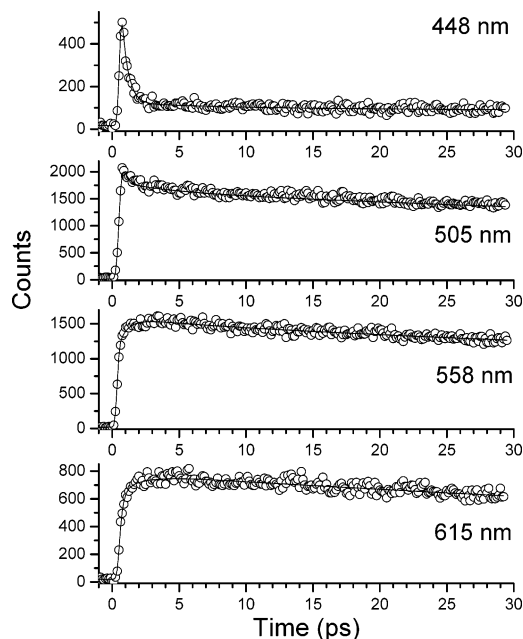*J. Phys. Chem. A, Vol. 109, No. 51, 2005* **11699**

Figure 4. Time-resolved sum frequency signal of fluorescence and gate pulse (760 nm) for **Ia** in acetonitrile. The solid lines express the corresponding best fitted curves.

Similar trends were observed in both solvents, in which the emission dynamics were nonsingly exponential. Detailed fitting parameters for both early-time relaxation dynamics and population decay rate at selected wavelengths are listed in Table 1. Upon monitoring at short wavelengths, the relaxation dynamics consist of a few hundred femtoseconds to a few picoseconds and a rather long (≫100 ps) decay component that can be treated as a constant value within the fitted range of < 30 ps. This long population decay component was further resolved to be 0.8 and 4.2 ns in CH_2Cl_2 and CH_3CN, respectively, via the ps/ns time-correlated single photon counting technique.

The short decay components (a few hundred femtoseconds to a few picoseconds) require at least two, and for some medium wavelengths even three, exponential terms to achieve good convoluted fits. For simplicity, Table 1 lists no more than two decay components. Upon increasing the monitored wavelength, while the population decay remains unchanged, the decay time of the early (fast) components gradually increases, accompanied by a decrease in the magnitude, and finally becomes a rise component at the very red edge of the emission. In this region, the best fitted time constants for the fast decay and/or rise components also vary by the probed emission wavelengths. To clearly map the above results, a temporal spectral evolution for the emission of **Ia** in CH_2Cl_2 was reconstructed; the results depicted in Figure 5 reveal a continuous spectral shift in fluorescence peak maxima, being red-shifted from the 430 nm at ~250 fs to ~465 nm at, for example, e.g. 3 ps. At >5 ps, the time-resolved spectrum remains nearly unchanged and its feature is the same as that obtained from the steady-state approach. The continuous spectral temporal evolution firmly supports the conclusion from the steady-state approach in that, upon Franck Condon excitation, the instant dipolar change in **Ia** should be quite large, as supported by the steady-state approach (16.9 D, vide supra), and can thus be treated as a charge-transfer process incorporating diethylamine (donor) and carbonyl oxygen (acceptor). The coupling between locally excited and charge-transfer states must be rather strong so that the solvent-polarization-induced barrier is negligible, and the entire process can be treated as an adiabatic type of optical

electron transfer. As a result, the relaxation dynamics of **Ia** are mainly governed by the solvation process, resulting in the salient time-dependent Stokes-shifted emission.

Relaxation Dynamics in I. For **I** in cyclohexane, the time-resolved trace (see Figure 6) at the very blue side, e.g., 427 nm, which is negligibly small in intensity and is ascribed to the normal emission in the steady-state measurement (see insert of Figure 1A), can be best fitted by two fast single-exponential decay components with a lifetime of 0.3 ps (46.4%) and 1.6 ps (53.6%) (see Table 1). Since these two values are very close, considering the system response of ~180 fs, within experimental error, a single-exponential fit of 1.53 ps ($\chi^2 \sim 1.17$) seems to be acceptable. When the wavelength was monitored at the proton-transfer tautomer emission, e.g. >600 nm, this fast decay component eventually disappeared and became a rise component with a rise time of ~1.5 ps, followed by a long population decay that can be treated as a constant in an acquisition period of ~25 ps. The long population decay was further resolved to be ~1.4 ns (see Table 1). The rise of the tautomer emission correlates well with the decay dynamics of the normal species, suggesting a precursor−sater type of relationship between normal (charge transfer) and proton-transfer tautomer emission, with a PT time of 1.5 ps.

Figures 7 and 8 depict the time-resolved traces of **I** in CH_2Cl_2 and CH_3CN, respectively. Detailed fitting parameters for early-time relaxation dynamics and population decay rates are listed in Table 1. In CH_2Cl_2, upon monitoring at short wavelengths, e.g. <450 nm, ascribed to the charge-transfer emission, the relaxation dynamics of **I** consist of a fast decay (less than a few picoseconds) (component 1) and a relatively slow decay component of ~110 ps (component 2). Both dynamics and amplitude of component 1 are wavelength dependent. On one hand, it requires at least two, and for some medium wavelengths even three, exponential terms to achieve good convoluted fits. For simplicity, Table 1 lists no more than two decay components. On the other hand, upon increasing the monitored wavelength, the amplitude of component 1 gradually decreases and becomes a rise component. Component 2 is well fitted by a single-exponential decay with a lifetime of ~120 ps in CH_2Cl_2 and it also gradually becomes a rise component upon increases of the monitoring wavelength, especially toward the red edge of the proton-transfer tautomer emission. For example, with monitoring at the proton-transfer tautomer region, e.g. 602 nm, a fast rise component of less than a few picoseconds was resolved, followed by a ~120 ps rise component and a rather long population decay component that was further resolved to be 3.4 ns via the ps/ns time correlated single-photon counting system. Obviously, the rise components of < few ps and ~120 ps monitored at proton-transfer tautomer emission correlate well with the fast (component 1) and ~110 ps decay components monitored at the charge-transfer emission.

Similar results were obtained for **I** in CH_3CN, consisting of a very fast decay (few hundred femtoseconds) component 1, a relatively slow (wavelength-dependent rise/decay) component 2, and a rather long population decay component (component 3) that appears upon monitoring at the proton-transfer emission band. Analogous to that in CH_2Cl_2, component 1 requires at least two, and for some medium wavelengths even three, exponential terms to achieve a good convoluted fit. Similarly, this fast decay becomes a rise component at longer emission wavelength. Note that component 2 in CH_3CN is much longer than that in CH_2Cl_2 and cannot be resolved by the fluorescence upconversion method. As shown at the bottom frame of Figure 8, both component 2 and component 3 were further resolved to

TABLE 1: Photophysical Properties of I and Ia in Various Solvents

solvent	emission[a] (Φ)	dynamics
		Compound **I**
cyclohexane	N: 405 nm	427 nm [τ_1: 0.30 ps(0.464), τ_2: 1.6 ps(0.536)]
	T: 560 nm (0.24)	560 nm [τ_1: 0.14 ps($-$0.076), τ_2: 1.7 ps ($-$0.428), τ_3: 1.40 ns (0.496)]
		602 nm [τ_1: 0.18 ps($-$0.066), τ_2: 1.5 ($-$0.417), τ_3: 1.42 ns (0.517)]
benzene	N: 425 nm	427 nm [τ_1: 0.96 ps(0.244), τ_2: 7.4 ps(0.756)]
	T: 566 nm (0.28)	560 nm [τ_1: 0.46 ps($-$0.108), τ_2: 7.2 ps ($-$0.370), τ_3: 2.0 ns (0.522)]
		602 nm [τ_1: 0.54 ps($-$0.116), τ_2: 7.0 ps($-$0.364), τ_3: 2.1 ns (0.520)]
dichloromethane	N: 460 nm	427 nm [τ_1: 1.76 ps(0.51), τ_2: 0.11 ns(0.49)]
	T: 564 nm (0.46)	565 nm [τ_1: 1.7 ps ($-$0.189), τ_2: 0.11 ns ($-$0.709), τ_3: 3.25 ns (0.101)]
		602 nm [τ_1: 2.3 ps($-$0.066), τ_2: 0.12 ns ($-$0.076), τ_3: 3.4 ns (0.858)]
acetonitrile	N: 480 nm	450 nm [τ_1: 0.67 ps(0.593), τ_2: 0.33 ns(0.407)]
	T: 565 nm (0.28)	570 nm [τ_1: 0.38 ps($-$0.063), τ_2: 0.37 ns ($-$0.024), τ_3: 1.81 ns (0.913)]
		611 nm [τ_1: 0.77 ps($-$0.077), τ_2: 0.39 ns($-$0.395), τ_3: 1.78 ns (0.528)]
		Compound **Ia**
cyclohexane	409 nm (0.03)	τ: 0.07 ns
benzene	431 nm (0.04)	417 nm [τ_1: 4.2 ps(0.506), τ_2: 169 ps (0.494)]
		460 nm [τ_1: 0.24 ps($-$0.397), τ_2: 172 ps (0.603)]
		505 nm [τ_1: 1.23 ps($-$0.351), τ_2: 188 ps(0.649)]
		558 nm [τ_1: 4.2 ps($-$0.506), τ_2: 179 ps (0.494)]
dichloromethane	465 nm (0.11)	427 nm [τ_1: 2.65 ps(0.472), τ_2: 0.80 ns (0.528)]
		460 nm [τ_1: 0.59 ps(0.581), τ_2: 1.83 ps(0.039), τ_3: 0.76 ns (0.380)]
		505 nm [τ_1: 0.33 ps($-$0.079), τ_2: 2.2 ps($-$0.421), τ_3: 0.78 ns (0.500)]
acetonitrile	513 nm (0.29)	448 nm [τ_1: 0.46 ps(0.829), τ_2: 1.1 ps(0.057), τ_3: 4.2 ns(0.114)]
		505 nm [τ_1: 0.31 ps(0.436), τ_2: 1.31 ps (0.052), τ_3: 4.1 ns (0.512)]
		558 nm [τ_1: 0.23 ps($-$0.700), τ_2: 1.2 ps($-$0.044), τ_3: 4.13 ns (0.256)]
		615 nm [τ_1: 0.31 ps($-$0.129), τ_2: 1.0 ps($-$0.171), τ_3: 4.0 ns (0.700)]

[a] N: "normal" or "charge-transfer" state emission maxima, T: tautomer state emission maxima. Data in parentheses are the fitted pre-exponential factor.
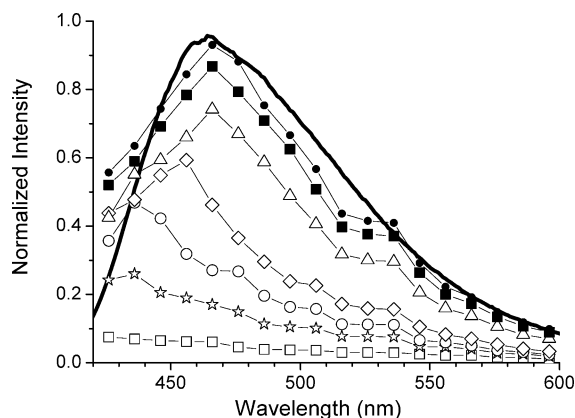

Figure 5. The temporal emission spectra of **Ia** in CH$_2$Cl$_2$ acquired at a delay time of: □: 250 fs, ☆: 375 fs, ○: 500 fs, ◇: 1 ps, △: 3 ps, ■: 5 ps, ●: 8 ps. The thick solid lines express the steady-state fluorescence.

be 390 ps and 1.78 ns with the time-correlated single photon-counting technique.

Due to the time scale of less than a few picoseconds as well as wavelength dependence, it seems reasonable to ascribe the origin of component 1 to the solvent relaxation dynamics. However, careful comparison of the early time-domain component 1 for **I** with respect to the solvent relaxation dynamics for **Ia** reveals several salient differences. For **I**, despite the wavelength-dependent decay rate of the major constituent of component 1, its time constant, under the same monitoring wavelength and detection condition, is always faster than the solvation dynamics obtained for **Ia**. For example, the ultrafast decay component at 427 nm was fitted to be 1.76 ps for **I** in CH$_2$Cl$_2$, which is nearly 1.5-folds as fast as that of 2.65 ps measured in **Ia** (see Table 1). Upon monitoring at a very red side of the tautomer emission, e.g. 602 nm, which is free from the charge-transfer emission, an ultrafast rise component of 2.3 ps was still resolved, with an initial population of ~7% (see
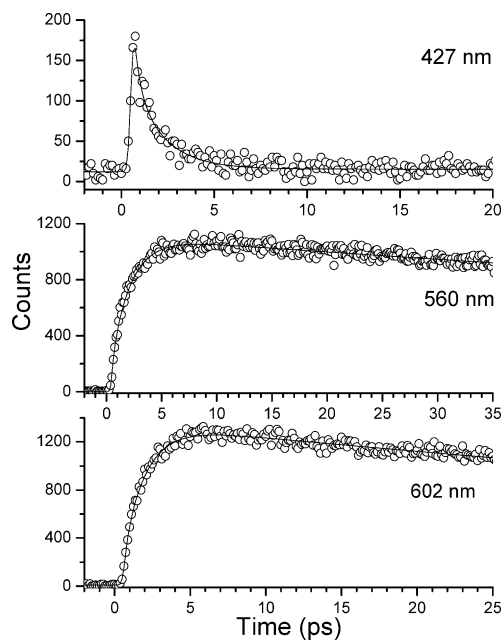

Figure 6. Time-resolved sum frequency signal of fluorescence and gate pulse (760 nm) for **I** in cyclohexane. The solid lines express the corresponding best fitted curves.

Scheme 2). Regarding the ultrafast population (7%) on the T* state, one possibility is the existence of equilibrium between N and T in the ground state, so that T* can be accessed via the direct Franck Condon excitation. However, this proposed mechanism is very unlikely since the theoretical calculation (HF/6-31G(d′,p′)//B3LYP/6-31G(d′,p′), see Experimental Section) estimates the energy difference between N(S$_0$) and T(S$_0$) to be as high as 11.46 kcal/mol. Apparently, in addition to the solvent relaxation channel, another ultrafast deactivation pathway in **I**, possibly incorporating the PT process, must play a key role to account for the observed early relaxation dynamics in polar aprotic solvents. As for component 2 in **I**, the good correlation
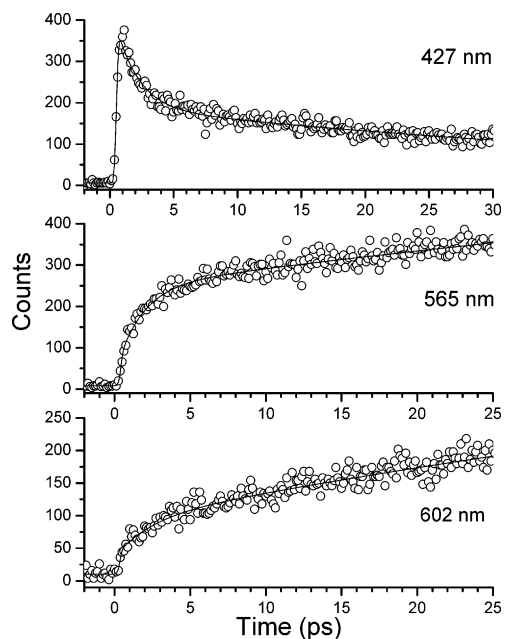
7-*N*,*N*-Diethylamino-3-hydroxyflavone

J. Phys. Chem. A, Vol. 109, No. 51, 2005 **11701**

Figure 7. Time-resolved sum frequency signal of fluorescence and gate pulse (760 nm) for **I** in dichloromethane. The solid lines express the corresponding best fitted curves.
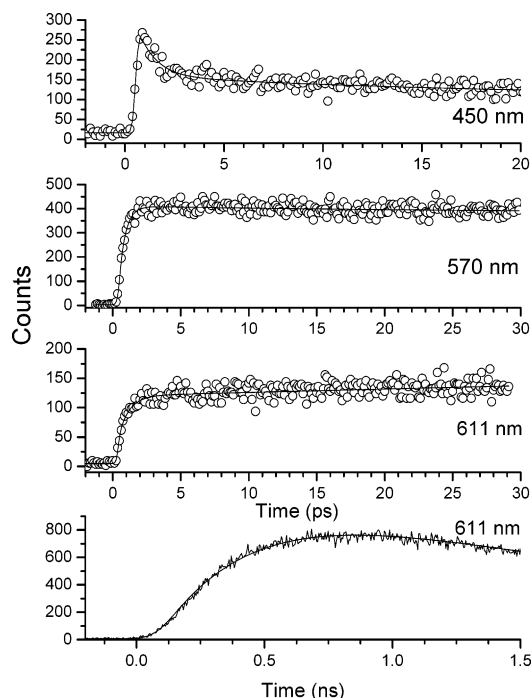

Figure 8. Time-resolved sum frequency signal of fluorescence and gate pulse (760 nm) for **I** in acetontrile. The solid lines express the corresponding best fitted curves. Note. The bottom time-resolved data was obtained using time-correlated single-photon counting technique.

between its decay in charge transfer emission and rise in the proton-transfer tautomer strongly supports the precursor (charge-transfer species) and successor (proton-transfer species) type of PT reaction. The rather slow time scale implies that the reaction is associated with an appreciable barrier, possibly induced by differences in equilibrium polarization between the charge transfer and proton transfer states (see the following section). Finally, due to the lack of a long population decay component (i.e., component 3 measured in the proton-transfer tautomer emission) upon monitoring at the charge-transfer emission band, even in the strongest polar solvent (CH_3CN)

SCHEME 2: The Proposed Relaxation Dynamics of I in, for Example, CH_3CN^a
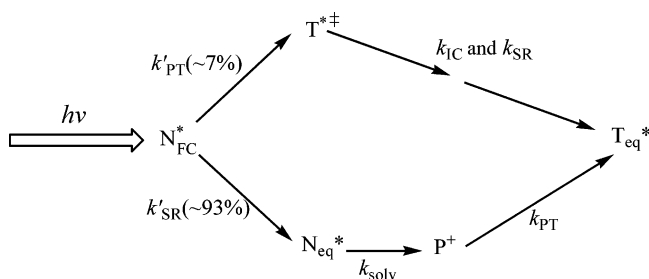
^{a} N_{FC}* represents the N → N* Franck−Condon excitation state. N_{eq}* and T_{eq}* are equilibrium configuration for N* and T*, respectively. T*‡ denotes the vibronically hot excited tautomer state. P$^+$ denotes the critical solvation configuration. k'_{PT} and k_{PT} are the rate constants of proton transfer at N_{FC}^+ and P$^+$, respectively. k'_{SR} and k_{SR} stand for rate constants of solvent relaxation, k_{IC} denotes the internal conversion, including the vibrational relaxation, k_{solv} represents the rate constant of solvent and nuclear reorganization prior to the proton-transfer reaction.

applied in this study, we conclude that that unlike the reversible type of PT in 4DHF,[15−19] PT (N* → T*) in **I** is highly exergonic and can thus be treated as an irreversible process.

4. Discussion

An essential requirement in rationalizing the above relaxation processes, i.e., components (1) and (2) simultaneously, is that N and T* must possess closer dipolar property, while the dipolar vector between N* and T* must be quite different due to the charge-transfer property in N* (vide infra). Accordingly, PT is energetically favorable at the Franck−Condon excited N*, N_{FC}*, and the associated rate is competitive with the rate of solvent relaxation. Upon reaching the equilibrium configuration in N*, denoted as N_{eq}*, slow PT takes place with appreciable barrier induced by the solvent polarity due to weakly coupled solvation potentials between N_{eq}* and T_{eq}*.

Perhaps the strongest support for the above viewpoint can be given by the spectral temporal evolution for **I**. As shown in Figure 9A, the time-dependent spectral evolution of **I** in CH_2-Cl_2, acquired at an earlier time domain, e.g. < 5.0 ps, revealed two distinct bands. The short wavelength band shifted from 430 to ∼470 nm upon increasing the pump−probe delay time from 250 fs to 5 ps. Note that the resulting 470 nm peak, within experimental uncertainty, is identical with the peak wavelength of the steady state charge transfer emission. Likewise, the 565-nm proton transfer emission band also gradually increases, while its peak wavelength is independent of the temporal evolution. The simultaneous growth for both charge transfer and tautomer emission at less than a few picoseconds unambiguously concludes the competitive solvation relaxation and PT processes. After a delay time of, e.g., > 25 ps, the 565-nm band continuously increases, together with a decrease of the 470 nm charge-transfer band (see Figure 9B). At a delay time of, for example, >500 ps, the time-resolved spectra are dominated by the 565 nm proton-transfer emission band, supporting the overall irreversible PT process.

The relatively slow PT time scale for component 2 (Figure 9B) implies that the reaction is associated with an appreciable barrier induced by differences in equilibrium polarization between N* and T*. To gain more detailed insight into the solvent-polarity-induced barrier, we therefore performed a temperature-dependent study to monitor the PT dynamics. Since this experiment focuses on the slow proton-transfer process (more than a few hundred picoseconds), the time-correlated
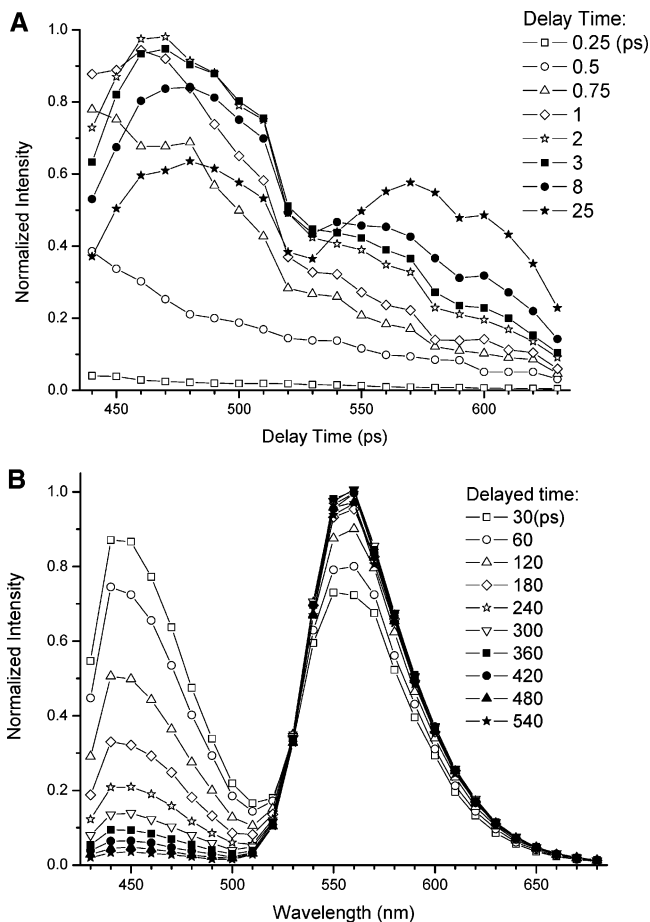
Figure 9. The temporal spectral evolution of **I** in CH_2Cl_2 acquired at a delay time of (A) 0.25−25 ps, (B) 30 to 540 ps. Each time interval in A and B is listed in the insert. Note that the results in A were obtained from the fluorescence upconversion experiment, while data for B were acquired with the time-correlated single photon counting technique.
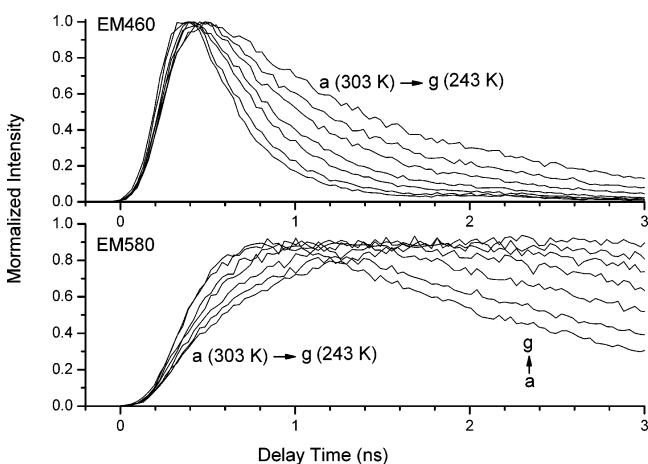

Figure 10. The temperature-dependent relaxation dynamics of **I** in CH_3CN monitored at 460 and 580 nm. Temperature ranges from a (303 K) to g (243 K) with a decrement of 10 K.

single photon counting technique with sub-nanosecond resolution is well suited for this study. Figure 10 shows the temperature-dependent decay and rise dynamics of **I** in CH_3-CN monitored at N* and T* emission bands, respectively. Clearly, as temperature decreases from 303 to 243 K, the decay time of the N* emission increases from 320 ps to 0.95 ns. Concurrently, the rise time of the T* emission increases from 360 ps to 1.05 ns, which, within experimental error, is consistent with the decay time monitored at the N* emission. The plot of
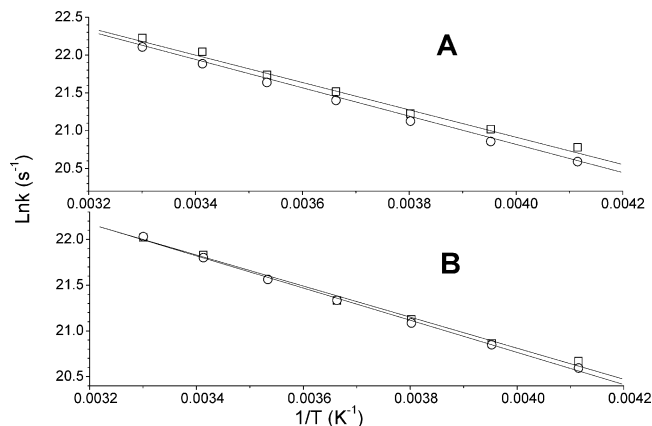

Figure 11. The temperature-dependent relaxation dynamics of **I** (−OH (□) and −OD (○)) in CH_3CN monitored at (A) 460 nm (decay component) and (B) 580 nm (rise component).

the decay rate constant (rise component) of the N* (T*) versus the reciprocal of temperature ($1/T$) reveals a straight line (Figure 11). Assuming that the quenching of N* population decay is dominated by PT, the results firmly support the N_{eq}* → T_{eq}* PT reaction in **I** to be a thermally activated process. More importantly, the rate of PT shows negligible kinetic isotope effect, as indicated by the identical straight line plot for the decay (rise) rate of N* (T*) emission versus $1/T$ between **I** (−OH) and **I** (−OD). The results clearly indicate that the rate along the proton migration coordinate is not a rate-determining factor; rather, the rate is mainly governed by a solvent-polarity-induced barrier. Taking the average deduced from the slope of decay (3.7 kcal/mol) and rise (3.5 kcal/mol) (Figure 11), a solvent-induced barrier of 3.6 kcal/mol is estimated in CH_3-CN. Note that this value is substantially higher than the viscosity barrier of <2.9 kcal/mol for CH_3CN at 298 K.[23] Thus, that the PT barrier originates from the perturbation of solvent polarity rather than the solvent viscosity is firmly supported.

To verify the relationships of dipolar vectors among the various states proposed above, we have thus performed theoretical approaches based on the 6-31G(d′,p′) basis sets at a Hartree−Fock level for both N and T. Conversely, the geometry of stationary points on the first electronic excited states was calculated using the CI Singles (CIS). Figure 12 depicts the structures of the lowest unoccupied (LUMO) and highest occupied (HOMO) frontier molecular orbitals mainly involved in the transition of the first excited states using the CIS//HF/6-31+G(d′,p′) method, the result of which predict that both N* and T* can be well ascribed using an allowed (π-symmetry) → π* (π-symmetry) transition. In the normal state, the contribution of lone pair electron density at the nitrogen atom is appreciable in HOMO, while it nearly vanishes in LUMO (see Figure 12). On the other hand, as shown in Figure 12, it is obvious that the electron density of carbonyl oxygen increases significantly from HOMO to LUMO. The result reaffirms the viewpoint of CT in **I** from diethylamine to the carbonyl oxygen. Furthermore, comparing to HOMO, the electron density in the carbonyl oxygen increases, while that of the hydroxyl group decreases in LUMO. The net result renders a driving force for the proton-transfer reaction in the excited state. Figure 13 depicts the magnitude and orientation of dipole vectors of **I** in ground and excited states for both normal and tautomer forms. The magnitudes of dipole moments for N and T were calculated to be 6.25 and 9.3 D, respectively, and the angle between these two dipole vectors was ∼20° (see Figure 13). Furthermore, the dipole moment of N* and T* were probed by the CIS/6-31G-(d′,p′) method. The results estimated a dipolar vector of 6.5 D
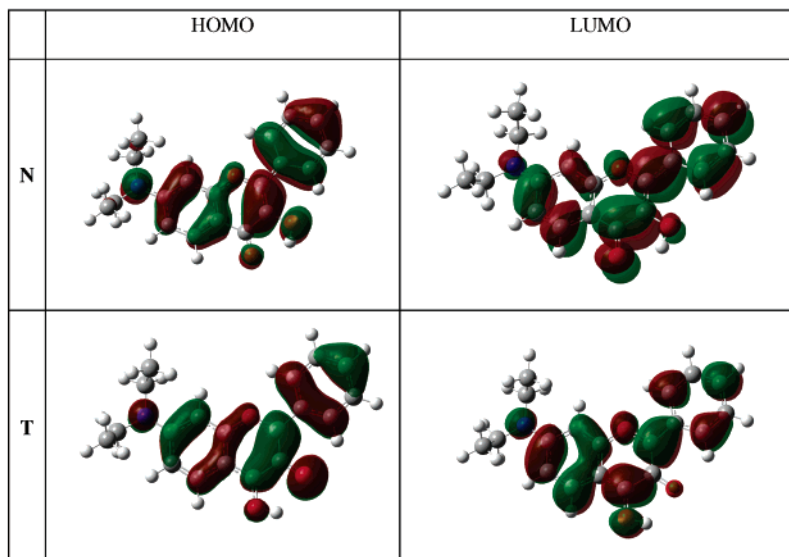
7-*N*,*N*-Diethylamino-3-hydroxyflavone

J. Phys. Chem. A, Vol. 109, No. 51, 2005 **11703**

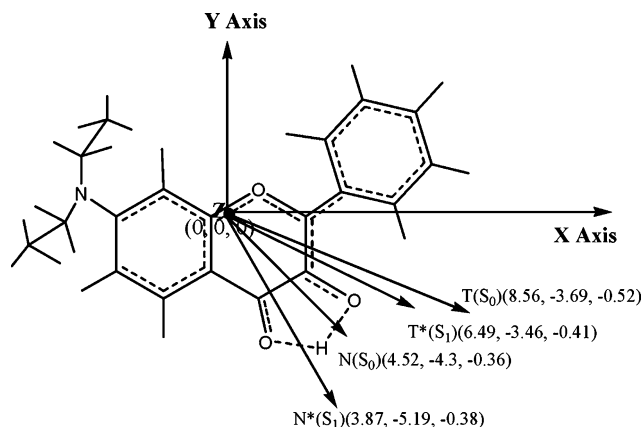**Figure 12.** The HOMO (π) and LUMO (π^*) of normal (N) and tautomer (T) species.

Figure 13. The magnitude and orientation of dipole vectors of **I** in ground and excited states for normal and tautomer forms. Note that the structure of **I** depicted here is a combination of normal and tautomer forms. The direction of *Z* axis in the Cartesian coordinates is perpendicular to this sheet. See Scheme 1 for clear structural visualization of N, N*, and T* (or T).

for N*, with an orientation of ~12° relative to that of N (see Figure 13). Though being a small change in magnitude, the substantial difference in dipole orientation between N and N* indicates a charge redistribution due to CT. Also, the calculation clearly revealed similar dipolar vectors between T (9.3 D) and T* (7.4 D), in which the angle between vectors of T and T* is as small as 5°, the result of which are consistent with experimental results of near solvent-polarity-independence for the proton-transfer tautomer emission peak. Another salient feature is in that the orientation difference in the dipolar vector between N* and T* (7.4 D) is as large as 25°. More importantly, as shown in Figure 13, the dipole vector of N lies between that of N* and T*.

Although the level and method used in the current theoretical approach are not high enough to ensure the quantitative values, the resulting correlations clearly show that N* and T* are subject to quite different solvent-polarization-modified free energy, while the solvent-polarization potential for N is expected to be between N* and T*. On this theoretical basis, we thus tentatively propose the overall excited-state relaxation pathways of **I** shown in Schemes 2 and 3 to rationalize the experimental results. Moreover, for the convenience of discussion, the relaxation pathway as a function of solvent polarities and reaction

SCHEME 3: The Proposed Relaxation Dynamics of I (in, for example, CH$_3$CN) as a Function of Solvent Polarities[a]
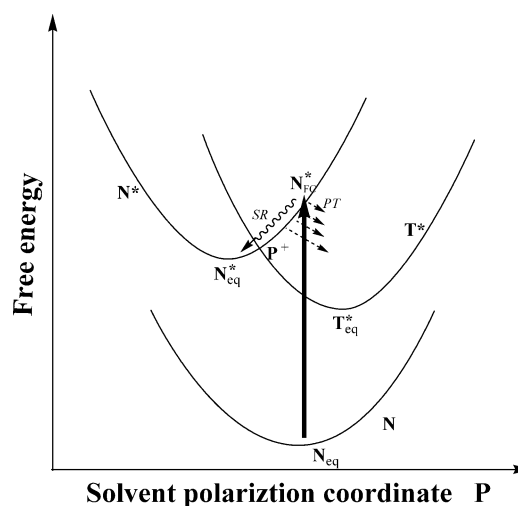
[a] See Scheme 2 for the definition of each term.

coordinates is also depicted in a 3D plot shown in Scheme 4. Upon Franck−Condon excitation (N$_{FC}$* in Schemes 2−4), **I** undergoes an instant dipolar change, mainly in the dipole orientation, due to an adiabatic type of CT. Thus, on one hand, solvent relaxation is expected to take place in N$_{FC}$*. On the other hand, because the polarization environment for N$_{FC}$* is between that of N* and T*, PT is energetically allowed (see Scheme 3) and its dynamics may be free from the solvent-polarity perturbation at early times. In other words, at N$_{FC}$* the solvent polarization effect may be decoupled between T* and N*, and the rate of intrinsic PT, as supported by the 1.5 ps^{-1} PT rate in cyclohexane (vide supra), should be fast, resulting in competitive deactivation pathways, i.e., PT versus solvent relaxation. As a result, such a fast proton transfer reaction gives rise to a vibronically hot tautomer denoted by T*† (see Scheme 2, upper pathway). T*† then undergoes internal conversion and possibly, in part, solvent relaxation pathways, resulting in a solvent equilibrated tautomer state T$_{eq}$* (see Schemes 2−4). In the other competitive pathway (see Scheme 2, lower pathway), due to the significant change in the dipole moment with respect to that of N$_{eq}$, N$_{FC}$*, also undergoes solvent relaxation to the

SCHEME 4: The Proposed Relaxation Dynamics of I (in, for example, CH₃CN) as a Function of Solvent Polarities and Reaction Coordinates in a 3-D Plot[a]
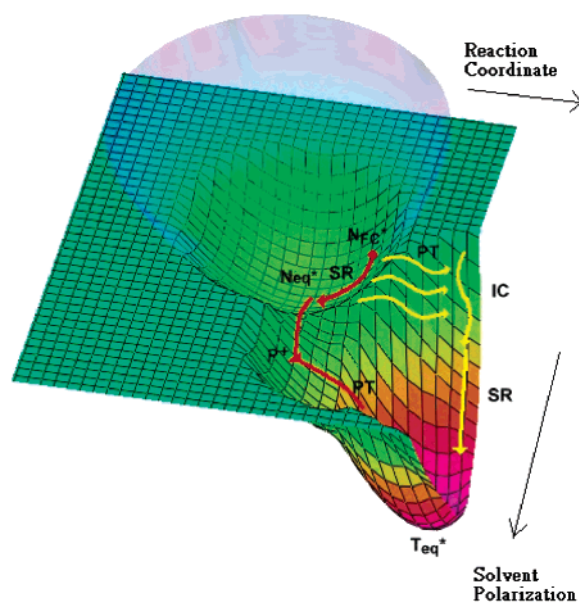
[a] IC denotes the internal conversion. See Schemes 2 and 3 for the detailed definition of other states and relaxation terms.

more stable solvation configuration. After reaching a critical solvation configuration, such as point P^+ depicted in Schemes 2−4, PT becomes energetically uphill due to the unfavorable solvent polarization, so the subsequent deactivation should be dominated by the solvent relaxation, finally reaching a solvent stabilized, equilibrated configuration N_{eq}^*. Because of the different equilibrium configurations between N_{eq}^* and T_{eq}^*, the solvent polarity effect is incorporated into the $N_{eq}^* \rightarrow T_{eq}^*$ PT reaction, resulting in an appreciable solvent polarity-induced barrier from N_{eq}^* to P^+, which is further deduced to be 3.6 kcal/mol from the temperature-dependent approach in CH₃CN. This $N_{eq}^* \rightarrow T_{eq}^*$ process can be ascribed as a typical Marcus−Weller type proton-transfer-coupled charge-transfer reaction. Another intriguing viewpoint worthy to note is regarding the pre-exponential factor of 1.8×10^{12} s⁻¹ in temperature-dependent rate expression. This value is in the same magnitude as the longitudinal relaxation time of CH₃CN ($\tau_L \sim 0.56$ ps).[24] The results indicate that proton transfer from the charge transfer to the proton-transfer tautomer species along the excited-state potential hypersurface occurs essentially every time the critical solvent configuration P^+ is achieved. In other words, the intrinsic proton-transfer rate, k_{PT}, at P^+ (see Scheme 2) is greater than the inverse of solvent longitudinal relaxation time (τ_L^{-1}). In this case, the pre-exponential A factor is approximately equal to τ_L^{-1} and is independent of the reactant/product coupling. Accordingly, despite a nonadiabatic type of solvent reorganization in the polarization coordinate for **I**, the intrinsic PT at P^+ may take place adiabatically along the reaction coordinate.

5. Conclusion

Comprehensive excitation behaviors of I have been investigated. We conclude that the relationship of dipole moments, and hence their associated solvent polarization potential, among N, N*, and T* is crucial to account for the observed relaxation dynamics. **I** possesses quite different dipolar characters in the N* and T* states, whereas that of N is in between. Thus, at the initial Franck−Condon excited-state N_{FC}^*, PT is energetically

favorable and is greatly decoupled from the solvent polarity effect. Its rate of ≤ 1 ps⁻¹ is competitive with the rate of N_{FC}^* $\rightarrow N_{eq}^*$ solvation relaxation. At the equilibrium configuration N_{eq}^*, despite the highly exergonic reaction pathway, the N_{eq}^* $\rightarrow T_{eq}^*$ is slow (less than a few tens of picoseconds) due to an appreciable barrier resulting from the solvent-polarity perturbation. Such fast and slow PT dynamics, in which the slow PT follows the conventional Marcus−Weller type of proton transfer-coupled electron transfer process, should be commonly observed in PT molecules with a similar relationship of dipolar vectors shown in Figure 13 and Scheme 3. The results not only add one more valuable prototype that fits in the category of proton-transfer-coupled charge-transfer systems, such as 2-hydroxy-4-(di-p-tolyl-amino)benzaldehyde[7] and 4'-N,N-dilkylamino-3-hydroxyflavones,[10−19] but also generalize the reaction dynamics based on the dipolar relationship among N, N*, and T*. We thus conclude that in polar, aprotic solvents such a relationship should be generally applied to many PT molecules to account for the observed early relaxation dynamics in polar, aprotic solvents.

6. Appendix

Synthesis. The synthetic scheme of **I** as well as their associated methoxy derivatives **Ia** is depicted in Scheme 5.

Preparation of 4-Diethylamino-2-methoxybenzaldehyde (1). A solution containing 4-diethylamino-2-hydroxybenzaldehyde (5.8 g, 30 mmol), KOH (2 g, 35 mmol), K₂CO₃ (8.3 g, 60 mmol), and dry CH₃CN (25 mL) was heated to 80 °C for 10 min with stirring. MeI (3.5 mL, 56 mmol) was then added to this alkaline solution, and the resulting mixture was stirred for 2 h at 80 °C. The reaction was cooled to room temperature followed by vacuum filtration. The filtrate was concentrated, and the residue was taken up in CH₂Cl₂ and washed with H₂O three times. The organic solution was dried over MgSO₄, concentrated under reduced pressure, and chromatographed on a silica gel column eluted with EtOAc/hexane (1:2 (v/v)) to afford **1** (5.5 g; 89%). Yellow solid, mp = 81−82 °C; TLC (EtOAc/hexane, 1:3) $R_f = 0.22$; ¹H NMR (400 MHz, CDCl₃) δ 10.08 (s, 1H), 7.66 (d, $J = 8.9$ Hz, 1H), 6.24 (d, $J = 8.9$ Hz, 1H), 6.00 (s, 1H), 3.85 (s, 3H), 3.39 (q, $J = 7.1$ Hz, 4H), 1.19 (t, $J = 7.1$ Hz, 6H); ¹³C NMR (100 MHz, CDCl₃) δ 187.03, 164.03, 153.77, 130.69, 114.10, 104.15, 92.29, 55.13, 44.73, 12.49; IR (KBr) 2971.9, 1647.4, 1590.1, 1526.1 cm⁻¹; FAB-MS: m/z 208.1 (M + H⁺), FAB−HRMS for C₁₂H₁₈NO₂ Calcd. 208.1337, Found 208.1337.

Preparation of 1-(4-Diethylamino-2-methoxyphenyl)ethanol (2). To the solution of compound **1** (5.5 g, 27 mmol) dissolved in 50 mL of dry THF was added 10 mL of MeMgCl dropwise at 0 °C, and the resulting solution was warmed to room temperature and maintained at this temperature for 1 h. A small amount of H₂O was added to decompose the excess of Grignard reagent, followed by removal of THF under reduced pressure. The residue was then taken up in CH₂Cl₂ and washed with H₂O three times. The organic phase was dried over MgSO₄ and concentrated. The residue was further purified by column chromatography on silica gel eluted with EtOAc/hexane (3:7 (v/v)) to afford **2** (5.4 g; 90%). Colorless viscous oil, TLC (EtOAc/hexane, 2: 3) $R_f = 0.32$; ¹H NMR (400 MHz, CDCl₃) δ 7.12 (d, $J = 8.4$ Hz, 1H), 6.25 (d, $J = 8.4$ Hz, 1H), 6.20 (s, 1H), 5.00 (q, $J = 6.5$ Hz, 1H), 3.83 (s, 3H), 3.33 (q, $J = 7.1$

SCHEME 5
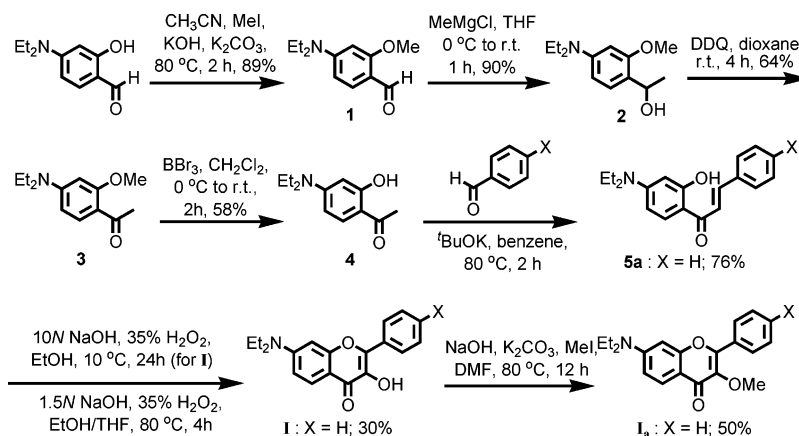
Hz, 4H), 2.57 (s, br, 1H), 1.47 (d, J = 6.5 Hz, 3H), 1.15 (t, J = 7.1 Hz, 6H); ^{13}C NMR (100 MHz, CDCl$_3$) δ 157.87, 148.44, 126.86, 120.44, 103.86, 95.20, 65.93, 55.02, 44.48, 22.52, 12.54; IR (naet) 3436.7, 2976.4, 2939.7, 1616.0, 1571.5, 1516.0, 1460.5 cm^{-1}; FAB-MS: m/z 223.1 (M$^+$), FAB−HRMS for C$_{12}$H$_{17}$NO$_2$ Calcd. 223.1573, Found 223.1573.

Preparation of 1-(4-Diethylamino-2-methoxyphenyl)etha-none (3). To a solution of DDQ (0.27 g, 1 mmol) in 2 mL of dioxane was added **2** (0.2 g, 0.9 mmol) in 2 mL of dioxane, and the resulting mixture was stirred at room temperature for 4 h. The mixture was filtered, and the solvent was evaporated under reduced pressure. The residue was purified by column chromatography on silica gel eluted with EtOAc/hexane (2:3 (v/v)) to afford **3** (130 mg; 64%). Greenish yellow solid, mp = 65−66 °C; TLC (EtOAc/hexane, 2: 3) R_f = 0.32; ^{1}H NMR (400 MHz, CDCl$_3$) δ 7.78 (d, J = 8.9 Hz, 1H), 6.29 (d, J = 8.9 Hz, 1H), 6.15 (s, 1H), 3.88 (s, 3H), 3.40 (q, J = 7.1 Hz, 4H), 2.52 (s, 3H), 1.20 (t, J = 7.1 Hz, 6H); ^{13}C NMR (100 MHz, CDCl$_3$) δ 196.15, 161.90, 152.59, 132.79, 115.84, 104.10, 93.66, 55.05, 44.56, 31.37, 12.52; IR (KBr) 2981.6, 1641.9, 1585.7, 1406.8 cm^{-1}; FAB-MS: m/z 222.1 (M + H$^+$), FAB−HRMS for C$_{13}$H$_{20}$NO$_2$ Calcd. 222.1494, Found 222.1485.

Preparation of 1-(4-Diethylamino-2-hydroxyphenyl)etha-none (4). To the solution of **3** (1.2 g, 5.4 mmol) in 25 mL of dry CH$_2$Cl$_2$ was cooled to −78 °C and followed by the addition of BBr$_3$ (0.6 mL; 6 mmol) predissolved in 5 mL of dry CH$_2$Cl$_2$ dropwise. The resulting solution was slowly warmed to room temperature and stirred continuously for 2 h. H$_2$O (10 mL) was added to the reaction mixture and followed by extraction with CH$_2$Cl$_2$ three times. The combined organic layers were dried over MgSO$_4$ and removed under reduced pressure, and the residue was purified by column chromatography on silica gel eluted with CH$_2$Cl$_2$/hexane (3:2 (v/v)) to afford **4** (650 mg; 58%). Colorless oil, TLC (CH$_2$Cl$_2$/hexane, 3:2) R_f = 0.25; ^{1}H NMR (400 MHz, CDCl$_3$) δ 12.89 (s, 1H), 7.49 (d, J = 9.1 Hz, 1H), 6.16 (dd, J = 9.1, 2.5 Hz, 1H), 6.05 (d, J = 2.5 Hz, 1H), 3.37 (q, J = 7.1 Hz, 4H), 2.45 (s, 3H), 1.18 (t, J = 7.1 Hz, 6H); ^{13}C NMR (100 MHz, CDCl$_3$) δ 200.28, 165.06, 153.76, 132.57, 109.76, 10.52, 97.04, 44.58, 25.42, 12.57; FAB-MS: m/z 208.2 (M + H$^+$), FAB−HRMS for C$_{12}$H$_{18}$NO$_2$ Calcd. 208.1338, Found 208.1332.

Preparation of 1-(4-Diethylamino-2-hydroxyphenyl)-3-phenylpropenone (5a). The title compound was prepared by the similar procedure reported in the literature.[25] A solution of **4** (3.5 g, 16 mmol), benzaldehyde (3 mL, 30 mmol), and ^{t}BuOK (4.4 g, 40 mmol), and 50 mL of dry benzene was stirred at 80 °C for 2 h. The reaction mixture was cooled to room temperature, poured into H$_2$O, and extracted with CH$_2$Cl$_2$ three times.

The combined organic layers were dried over MgSO$_4$ and concentrated under reduced pressure. The residue was purified by column chromatography on silica gel eluted with CH$_2$Cl$_2$/hexane (9:1 (v/v)) to afford **5a** (3.7 g; 76%). Orange solid, mp = 103−104 °C; TLC (CH$_2$Cl$_2$) R_f = 0.3; ^{1}H NMR (400 MHz, CDCl$_3$) δ 7.83 (d, J = 8.9 Hz, 1H), 7.70 (m, 2H), 7.58 (d, J = 7.3 Hz, 2H), 7.32 (m, 3H), 6.28 (dd, J = 8.9, 1.7 Hz, 1H), 6.08 (d, J = 1.7 Hz, 1H), 3.89 (s, 3H), 3.37 (q, J = 7.1 Hz, 4H), 1.17 (t, J = 7.1 Hz, 6H); ^{13}C NMR (100 MHz, CDCl$_3$) δ 188.14, 161.45, 152.37, 139.98, 135.87, 133.36, 129.22, 128.53, 127.86, 127.78, 116.14, 104.16, 93.43, 55.28, 44.44, 12.43; IR (KBr) 2975.2, 1645.4, 1608.4, 1576.2, 1405.7 cm^{-1}; FAB-MS: m/z 310.2 (M + H$^+$), FAB−HRMS for C$_{20}$H$_{24}$NO$_2$ Calcd. 310.1807, Found 310.1804.

Preparation of 7-*N,N*-Diethylamino-3-hydoxyflavone (I). The title compound was prepared by the similar procedure reported in the literature.[26] To a solution of **5a** (0.2 g, 0.68 mmol) in 4 mL of EtOH was added 1 mL of 10 N NaOH (0.4 g, 10 mmol) solution, and the resultant solution was stirred 10 min at 10 °C. The color of the solution slowly changed from red to dark red. At this moment, 35% H$_2$O$_2$ (0.4 mL, 4.7 mmol) was added to the solution, and the reaction was stir continuously for 24 h at 10 °C. The reaction mixture was then poured into water and acidified with 10% HCl, followed by extraction with CH$_2$Cl$_2$ three times. The combined organic layers were dried over MgSO$_4$ and concentrated under reduced pressure. The residue was purified by column chromatography on silica gel eluted with CH$_2$Cl$_2$ to afford **I** (63 mg; 30%). Yellow solid, mp = 153−154 °C; TLC (CH$_2$Cl$_2$) R_f = 0.25; ^{1}H NMR (400 MHz, CDCl$_3$) δ 8.19 (d, J = 7.5 Hz, 2H), 7.99 (d, J = 7.1 Hz, 1H), 7.48 (t, J = 7.5 Hz, 2H), 7.38 (t, J = 7.5 Hz, 1H), 7.11 (s, br, 1H), 6.73 (d, J = 7.1 Hz, 1H), 6.53 (s, 1H), 3.44 (q, J = 7.1 Hz, 4H), 1.23 (t, J = 7.1 Hz, 6H); ^{13}C NMR (100 MHz, CDCl$_3$) δ 158.17, 152.03, 142.83, 137.81, 131.84, 129.27, 128.35, 127.34 (*2), 126.59, 110.86, 110.53, 96.36, 44.79, 12.49; IR (KBr) 3274.8, 1286.6, 1613.4, 1594.9, 1523.5, 1417.5, 1355.3, cm^{-1}; FAB-MS: m/z 310.1 (M + H$^+$), FAB−HRMS for C$_{19}$H$_{20}$NO$_3$ Calcd. 310.1443, Found 310.1443.

Preparation of 7-*N,N*-Diethylamino-3-methoxyflavone (Ia). The reaction procedure is similar to the one used for the preparation of compound **1**. A mixture of **I** (0.4 g, 1.3 mmol), NaOH (0.1 g, 2.5 mmol), K$_2$CO$_3$ (0.3 g, 2.2 mmol), and 3 mL of dry DMF was heated to 80 °C and stirred for 10 min followed by the addition of MeI (0.1 mL, 1.6 mmol) to afford **Ia** (210 mg; 50%). Yellow solid, mp = 94−96 °C; TLC (EtOAc/CH$_2$-Cl$_2$, 1:9) R_f = 0.2; ^{1}H NMR (400 MHz, CDCl$_3$) δ 8.06 (m, 3H), 7.49 (m, 3H), 6.74 (dd, J = 8.8, 2.8 Hz, 1H), 6.51 (d, J = 2.8 Hz, 1H), 3.86 (s, 3H), 3.45 (q, J = 7.1 Hz, 4H), 1.23

11706 *J. Phys. Chem. A, Vol. 109, No. 51, 2005*

Cheng et al.

(t, J = 7.1 Hz, 6H); ^{13}C NMR (100 MHz, CDCl$_3$) δ 173.99, 157.56, 153.88, 151.49, 140.84, 131.31, 129.95, 128.24, 126.78, 113.52, 110.43, 96.12, 60.18, 44.88, 12.58; IR (KBr) 2971.1, 1631.0, 1590.4, 1531.4, 1452.2, 1396.9, 1355.8 cm^{-1}; FAB-MS: *m/z* 324.1 (M + H$^+$), FAB−HRMS for C$_{20}$H$_{22}$NO$_3$ Calcd. 324.1600, Found 324.1606.

References and Notes

(1) a) Scheiner, S. *J. Phys. Chem. A* **2000**, *104*, 5898. (b) Waluk, J. Conformational Aspects of Intra- and Intermolecular Excited-State Proton Transfer. In *Conformational Analysis of Molecules in Excited States*; Waluk, J., Ed.; Wiley-VCH: New York, 2000. (c) Chou, P. T. *J. Chin. Chem. Soc.* **2001**, *48*, 651. (d) Wu, K.-C.; Cheng, Y.-M.; Lin, Y.-S.; Yeh, Y.-S.; Pu, S.-C.; Hu, Y.-H.; Yu, J.-K.; Chou, P.-T. *Chem. Phys. Lett.* **2004**, *382,* 203. (e) Paterson, M. J.; Robb, M. A.; Blancafort, L.; DeBellis, A. D.; *J. Am. Chem. Soc.* **2004**, *126*, 2912. (f) Lochbrunner, S.; Wurzer, A. J.; Riedle, E. *J. Phys. Chem. A* **2003**, *107*, 10580. (g) de Vivie-Riedle, R.; De Waele, V.; Kurtz, L.; Riedle, E. *J. Phys. Chem. A* **2003**, *107*, 10591. (h) Shynkar, V. V.; Mely, Y.; Duportail, G.; Piemont, E.; Klymchenko, A. S.; Demchenko, A. P. *J. Phys. Chem. A* **2003**, *107*, 9522. (i) Cheng, C.-C.; Chang, C.-P.; Yu, W.-S.; Hung, F.-T.; Liu, Y.-I.; Wu, G.-R.; Chou, P.-T. *J. Phys. Chem. A* **2003**, *107*, 1459. (j) Lukeman, M.; Wan, P. *J. Am. Chem. Soc.* **2003**, *125*, 1164.

(2) In some PT molecules, the lowest excited singlet state is in an nπ* configuration, in which PT is prohibited. For the relevant review, see ref 1a.

(3) PT incorporating phenol O−H to a β-carbon atom is not included in this category, see: Lukeman, M.; Wan, P. *J. Am. Chem. Soc.* **2002**, *124*, 9458.

(4) For example, see: (a) Schwartz, B. J.; Peteanu, L. A.; Harris, C. B. *J. Phys. Chem.* **1992**, *96*, 3591. (b) Chudoba, C.; Riedle, E.; Pfeiffer, M.; Elsaesser, T. *Chem. Phys. Lett.* **1996**, *263*, 622.

(5) Lochbrunner, S.; Wurzer, A. J.; Riedle, E. *J. Chem. Phys.* **2000**, *112*, 10699.

(6) Chou, P.-T.; Huang, C.-H.; Pu, S.-C.; Cheng, Y.-M.; Liu, Y.-H.; Wang, Y.; Chen, C.-T. *J. Phys. Chem. A* **2004**, *108*, 6452.

(7) Chou, P.-T.; Yu, W.-S.; Cheng, Y.-M.; Pu, S.-C.; Yu, Y.-C.; Lin, Y.-C.; Huang, C.-H.; Chen, C.-T. *J. Phys. Chem. A* 2004, 108, 6487.

(8) Kim, Y.; Yoon, M.; Kim, D. *J. Photochem. Photobiol. A: Chemistry* **2001**, *138*, 167.

(9) Paterson, M. J.; Robb, M. A.; Blancafort, L.; DeBellis, A. D. *J. Am. Chem. Soc.* **2004**, *126*, 2912.

(10) Chou, P.-T.; Martinez, M. L.; Clements, J. H. *J. Phys. Chem.* **1993**, *97*, 2618.

(11) Chou, P.-T.; Martinez, M. L.; Clements, J. H. *Chem. Phys. Lett.* **1993**, *204*, 395.

(12) Swinney, T. C.; Kelley, D. F. *J. Chem. Phys.* **1993**, *99*, 211.

(13) Parsapour, F.; Kelley, D. F. *J. Phys. Chem.* **1996**, *100*, 2791.

(14) Ormson, S. M.; Brown, R. G.; Vollmer, F.; Rettig, W. *J. Photochem. Photobiol. A* **1994**, *81*, 65.

(15) Ameer-Beg, S.; Ormson, S. M.; Poteau, X.; Brown, R. G.; Foggi, P.; Bussotti, L.; Neuwahl, F. V. R. *J. Phys. Chem. A* **2004**, *108*, 6938.

(16) Douhal, A.; Sanz, M.; Carranza, M. A.; Organero, J. A.; Santos, L. *Chem. Phys. Lett.* **2004**, *394*, 54.

(17) Chou, P. T.; Pu, S. C.; Cheng, Y. M.; Yu, W. S.; Yu, Y. C.; Hung, F. T.; Hu, W. P. *J. Phys. Chem. A* **2005**, *109*, 3777.

(18) Roshal, A. D.; Organero, J. A.; Douhal, A. *Chem. Phys. Lett.* **2003**, *379*, 53.

(19) Shynkar, V. V.; Mely, Y.; Duportail, G.; Piemont, E.; Klymchenko, A. S.; Demchenko, A. P. *J. Phys. Chem. A* **2003**, *107*, 9522.

(20) Chou, P.-T.; Chen, Y.-C.; Yu, W.-S.; Chou, Y.-H.; Wei, C.-Y.; Cheng, Y.-M. *J. Phys. Chem. A* **2001**, *105*, 1731.

(21) Frisch, M. J.; Trucks, G. W.; Schlegel, H. B.; Scuseria, G. E.; Robb, M. A.; Cheeseman, J. R.; Montgomery, J. A., Jr.; Vreven, T.; Kudin, K. N.; Burant, J. C.; Millam, J. M.; Iyengar, S. S.; Tomasi, J.; Barone, V.; Mennucci, B.; Cossi, M.; Scalmani, G.; Rega, N.; Petersson, G. A.; Nakatsuji, H.; Hada, M.; Ehara, M.; Toyota, K.; Fukuda, R.; Hasegawa, J.; Ishida, M.; Nakajima, T.; Honda, Y.; Kitao, O.; Nakai, H.; Klene, M.; Li, X.; Knox, J. E.; Hratchian, H. P.; Cross, J. B.; Bakken, V.; Adamo, C.; Jaramillo, J.; Gomperts, R.; Stratmann, R. E.; Yazyev, O.; Austin, A. J.; Cammi, R.; Pomelli, C.; Ochterski, J. W.; Ayala, P. Y.; Morokuma, K.; Voth, G. A.; Salvador, P.; Dannenberg, J. J.; Zakrzewski, V. G.; Dapprich, S.; Daniels, A. D.; Strain, M. C.; Farkas, O.; Malick, D. K.; Rabuck, A. D.; Raghavachari, K.; Foresman, J. B.; Ortiz, J. V.; Cui, Q.; Baboul, A. G.; Clifford, S.; Cioslowski, J.; Stefanov, B. B.; Liu, G.; Liashenko, A.; Piskorz, P.; Komaromi, I.; Martin, R. L.; Fox, D. J.; Keith, T.; Al-Laham, M. A.; Peng, C. Y.; Nanayakkara, A.; Challacombe, M.; Gill, P. M. W.; Johnson, B.; Chen, W.; Wong, M. W.; Gonzalez, C.; Pople, J. A. *Gaussian 03*, revision C.02; Gaussian, Inc.: Wallingford, CT, 2004.

(22) Foresman, J. B.; Head-Gordon, M. People, J. A.; Frish, M. J. *J. Phys. Chem.* **1992**, *96*, 135.

(23) Brucker, G. A.; Swinney, T. C.; Kelly, D. F. *J. Phys. Chem.* **1991**, *95*, 3190.

(24) Kahlow, M. A.; Jarzeba, W.; Kang, T. A.; Barbara, P. F. *J. Chem. Phys.* **1989**, *90*, 151.

(25) Murafuji, T.; Sugihara, Y.; Moriya, T.; Mikata, Y.; Yano, S. *New J. Chem.* **1999**, *23*, 683.

(26) Smith, M. A.; Neumann, R. M.; Webb, R. A. *J. Heterocycl. Chem.* **1968**, *5*, 425. (b) Hsu, K. K.; Shi, J. Y. *J. Chin. Chem. Soc.* **1973**, *20*, 51. (c) Meyer, N. D.; Haemers, A.; Mishra, L.; Pandey, H.-K.; Pieters, L. A. C.; Derghe, D. A. V.; Vlietinck, A. J. *J. Med. Chem.* **1991**, *34*, 736